Ceramics International 42 (2016) 16710–16717

Contents lists available at ScienceDirect

Ceramics International

journal homepage: www.elsevier.com/locate/ceramint

Innovative preparation route for uranium carbide using citric acid as a carbon source

D. Salvato [a,b], J.-F. Vigier [a,*], O. Dieste Blanco [a], L. Martel [a], L. Luzzi [b], J. Somers [a], V. Tyrpekl [a,**]

[a] European Commission, Joint Research Centre (JRC), Institute for Transuranium Elements (ITU), Postfach 2340, Karlsruhe 76125, Germany
[b] Politecnico di Milano, Department of Energy, CeSNEF (Enrico Fermi Center for Nuclear Studies), via La Masa 34, Milano 20156, Italy

ARTICLE INFO

Article history:
Received 30 May 2016
Received in revised form
13 July 2016
Accepted 20 July 2016
Available online 21 July 2016

Keywords:
Uranium carbide
Citric acid
Carbothermal reduction
Spark plasma sintering

ABSTRACT

The preparation of uranium carbide (UC) by carbothermal reduction and its sintering into dense pellets by conventional means require high temperatures for long periods. We have developed a preparation route yielding fine UC powder with significantly increased sinterability. At first, a mixture of nanocrystalline UO_2 embedded in amorphous carbon (nano-UO_2/C) was obtained by thermal decomposition of a gel containing solubilised uranyl nitrate and citric acid. Later, the nano-UO_2/C powder was treated in a conventional furnace or in a modified spark plasma sintering facility at elevated temperatures ($\geq$ 1200 °C) in order to obtain uranium carbide powder. The effects of initial composition, temperature, gas/vacuum atmosphere and the overall reaction kinetics are reported.

1. Introduction

Uranium and mixed uranium-plutonium carbides are considered as fuels for fast breeder reactors. Recently, comprehensive reviews of the use of carbide fuels [1] and their thermophysical properties [2] have been published.

Typically, the preparation of U(Pu)C involves UO_2 (PuO_2) powder mixing and blending with graphite or carbon black followed by carbothermal reduction (CTR, Eqs. ((1), 2)) at temperatures above 1500 °C for several hours [2,3]:

$$UO_2+4C \rightarrow UC_2+2CO \quad (1)$$

$$UO_2+3UC_2 \rightarrow 4UC+2CO \quad (2)$$

For example, Suzuki et al. [4] used a UO_2, PuO_2 and graphite powder mixture (molar ratio of $C/(UO_2+PuO_2)=2.975$) that was ball-milled for 48 h. The CTR proceeded at 1500 °C for 4 h. The results showed that all the powder contained a minor $UPuO_{2-x}$ phase, whatever the atmosphere (0.2, 10^{-3} Pa or He) employed. Moreover, the powder had to be ball-milled again before pressing and sintering. Ganguly et al. [5] ball-milled UO_2, PuO_2 and a graphite mixture for 12 h, compacted at 105 MPa and performed CTR at 1475 °C for 4 h at 1 kPa. The powder contained 10–15 wt% U $(Pu)_2C_3$ and up to 0.45 wt% oxygen. Duguay and Pelloquin [6] used a similar procedure: blending, milling, pressing and CTR at 1500–1750 °C for 15 h under vacuum, with a oxide/carbon ratio of 3.09. Vaudez et al. [7] used the same process, while setting the CTR conditions to 1550 °C for 15 h.

All the above investigations can be considered as "conventional" carbide preparation routes, which use an oxide/graphite blend as a starting material. Recently, a big step has been taken in the preparation of non-nuclear carbides. Organic species are used as a source of fine carbon with high surface area consequently leading to milder conditions needed for the CTR. For example, Matović et al. [8], Yan et al. [9] and Lu et al. [10] reported the synthesis of HfC using citric acid as a carbon source. Similarly, citric acid was used for the preparation of VC [11], B_4C [12] or WC [13]. Apart from citric acid other organic compounds may be used as a carbon source, for example chitosan [14], ascorbic acid [15], phenolic resin [16,17] or divinylbenzene [18].

In this work, we describe a preparation of uranium carbide derived from a solution of uranyl nitrate and citric acid. Uranyl cation forms a 1:1 complex $[UO_2(cit)]^-$ with the citrate at pH $\leq$ 1, while at higher pH the molecules start to form a dimer $[(UO_2)_2(cit)_2]^{2-}$ bridged by the alcohol group of the citric acid [19,20]. Complexation of the uranyl ion assures a perfect homogenous distribution of the carbon and the metal source. This solution is decomposed by increasing the temperature to 1000 °C in Ar to form nanocomposite UO_2/C. Suzuki et al. [21] performed a

* Corresponding author.
** Corresponding author. Current address: Belgian Nuclear Research Centre SCK · CEN, Boeretang 200, Mol, Belgium.
E-mail addresses: jean-francois.vigier@ec.europa.eu (J.-F. Vigier), vaclav.tyrpekl@sckcen.be (V. Tyrpekl).

http://dx.doi.org/10.1016/j.ceramint.2016.07.138

kinetic study on CTR and identified the most limiting factors as the oxygen diffusion in UO_2 particles at the reaction interphase or the diffusion of CO gas through a compact layer. This can be overcome by nanocomposite UO_2/C due to the high interface area and interconnected porosities after citrate decomposition. The nanocomposite is then treated at elevated temperatures ($\geq$ 1200 °C) in a spark plasma sintering (SPS) apparatus devoted to radiotoxic materials [22], which was modified for CTR purposes similarly as in Feng et al. [23].

2. Experimental part

2.1. Materials and preparation

The preparation route can be divided into several steps as presented in the flowchart of Fig. 1:

(1) Uranyl nitrate and citric acid (Alfa Aesar, 99%) solutions were mixed in desired molar ratios.

(2) The solution was treated with the following decomposition program under Ar atmosphere – heating at 50 °C/h to 200 °C with no dwell time; from 200 to 1000 °C at 200 °C/h and a 1 h dwell; cooling at 200 °C/h to room temperature. The resulting powder was crushed and homogenized in a mortar, and was denoted as "nanocrystalline UO_2/C". Two options may follow, either CTR in a conventional furnace (3A) or in the modified spark plasma sintering facility (3B).

(3A) Nanocrystalline UO_2/C powder was introduced into a conventional metallic furnace at 1600 °C under argon flow with a 1 h dwell (heating and cooling ramps at 200 °C/h), where the CTR took place.

(3B) Nanocrystalline UO_2/C powder was hand-pressed into a modified SPS die and the CTR was conducted under vacuum in the modified SPS (described in the following subsection 2.2.).

From the step (2), powders manipulations were done in glove boxes designed for radioactive materials handling under inert atmosphere (nitrogen or argon). The water content in the glove boxes atmosphere is generally less than 10 ppm, but O_2 content can rise up to 0.7%.

2.2. Spark plasma sintering device adapted for CTR

Spark plasma sintering in its normal configuration belongs to the group of electric field assisted sintering techniques. Normally, it is used to simultaneously press and sinter compacts using graphite dies and punches. Here, the classical set-up was modified so that it can be used as pressureless furnace as shown in Feng et al. [23]. Fast heating and cooling ramps that prevent grain growth and necking are the advantages of this special use of the SPS, thus the resulting powder has increased sinterability. The SPS facility (FCT Systeme GmbH, Rauenstein, Germany) is described in [22]. The graphite set-up used for CTR is presented in Fig. 2. The main innovation is the annular punch fitted with a horizontal orifice to permit the fast CO release thanks to vacuum in SPS chamber. Use of the conventional SPS arrangement resulted in a quasi-sealed containment, which did not permit CO release. In this case there is no carbothermal reaction at all, confirming Suzuki's hypothesis [21]. The typical heating cycle was – heating ramp at 200°C/min to the desired temperature (1200, 1400, 1600°C), desired dwell (0, 5, 10, 20, 30min) with a cooling ramp of 200°C/min to room temperature.

2.3. Analytical techniques

2.3.1. Powder X-ray diffraction

The structure of the products was determined at room temperature by X-ray diffraction (XRD) using a Bruker D8 X-ray diffractometer mounted in a Bragg–Brentano configuration with a curved Ge monochromator (1, 1, 1) and a ceramic copper tube (40 kV, 40 mA) equipped with a LinxEye position sensitive detector. For the measurement, the powder was deposited on a silicon wafer to minimize the background and dispersed on the surface with 2 or 3 drops of isopropanol. Structural analyses were performed by the Rietveld method with the JANA 2006 software [24].

2.3.2. ^{13}C nuclear magnetic resonance

^{13}C Magic Angle Spinning Nuclear Magnetic Resonance (MAS NMR) experiments were performed at 100 MHz on a Bruker 9.4T dedicated for the study of radioactive materials [25]. A 4 mm probe was used and the sample spun at 10 kHz. A Hahn echo sequence was performed with 90° and 180° pulse lengths of 8.2 µs and 16.4 µs respectively with an echo delay of 1 rotor period. A recycle delay of 500 ms was used. The sample was referenced to tetramethysilane (0 ppm). The spectrum was fitted using the dmfit software [26].

2.3.3. Electron microscopy

Crystallite size and morphology of the samples were studied using a transmission electron microscope (TEM) TecnaiG2 (FEI™) 200 kV equipped with a field emission gun, modified during its construction to enable the examination of radioactive samples. The TecnaiG2 TEM is equipped with a Gatan™ Tridiem GIF camera, an energy-dispersive X-ray (EDX) analysis system, and a high-angle annular dark-field (HAADF) detector for the scanning transmission electron microscope (STEM) imaging. The samples for the TEM investigations were prepared by crushing tiny fragments of

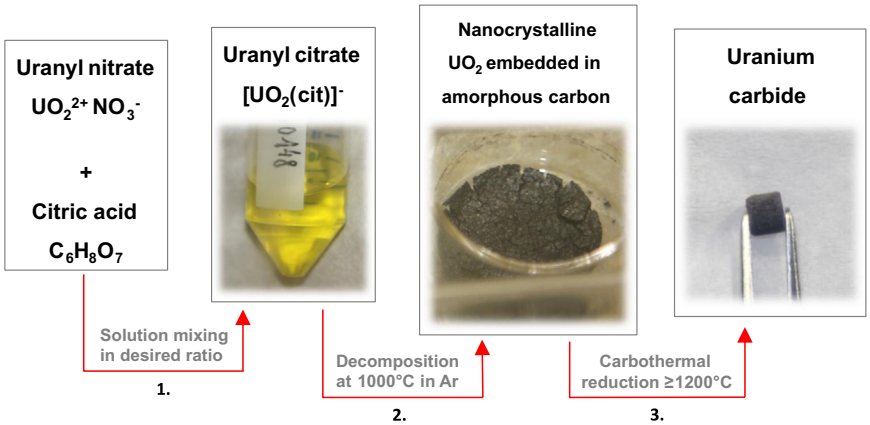

Fig. 1. Flowchart representing the preparation steps for uranium carbide starting from uranyl nitrate and citric acid solutions.

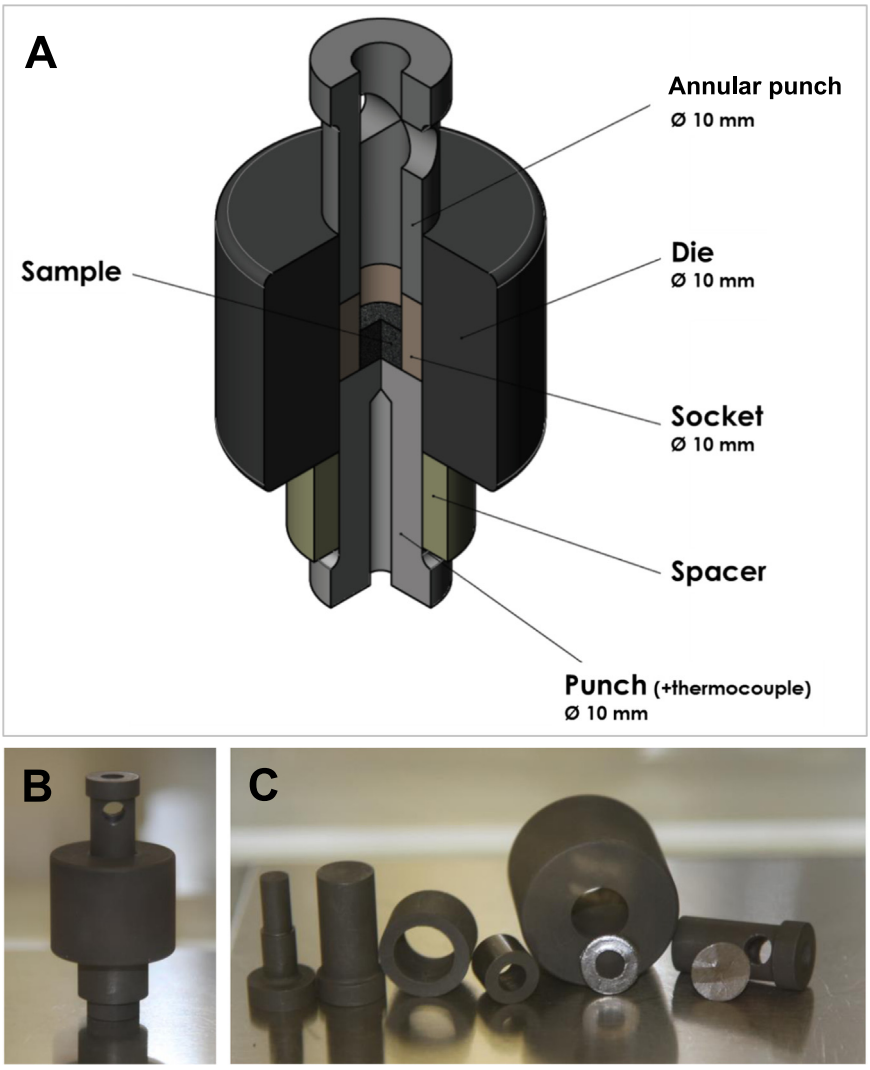

Fig. 2. Technical drawing of the SPS die and punches modification for CTR purposes (A), photography of the assembled (B) and disassembled (C) set-up.

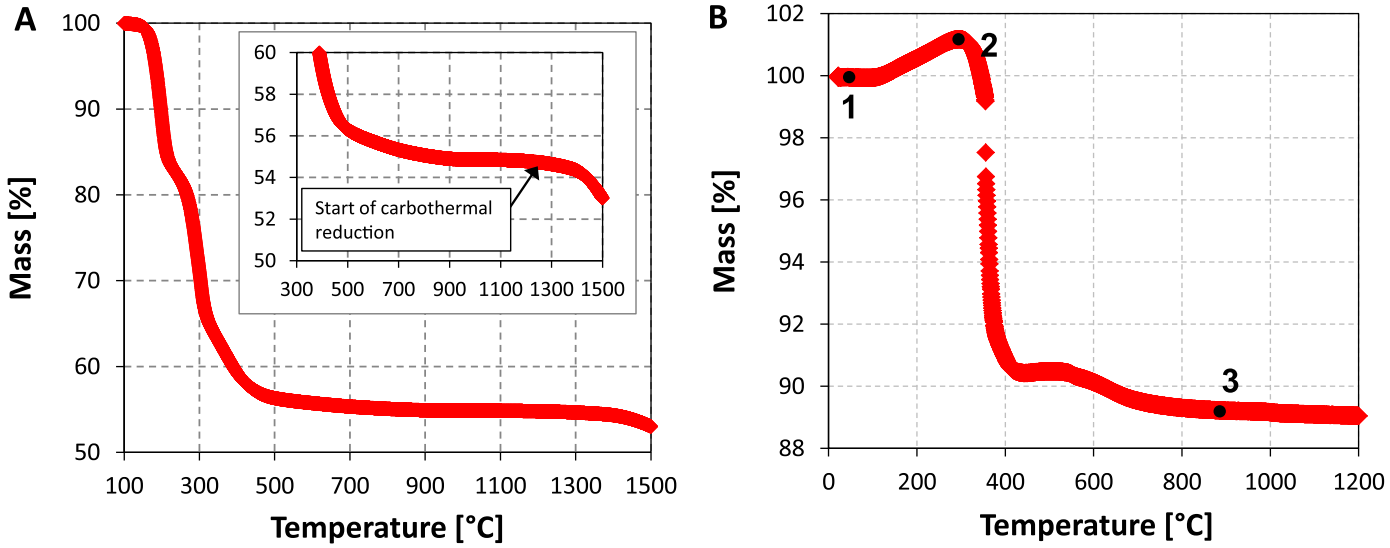

Fig. 3. Thermogravimetric study of the mixed uranyl nitrate and citric acid solutions dried at 150°C for 2h, the citrate/UO_2^{2+} molar ratio is 2.0. Decomposition in Ar with a heating ramp of 10°C/min. The start of the CTR is observable around 1200°C (A) Oxidation study in air of the nanocrystalline UO_2/C composite showing UO_2-U_3O_8 oxidation (1→2) and burning of carbon (2→3) (B).

the various compounds in methanol. The resulting suspension was allowed to stand for decanting, and a droplet subsequently deposited on a copper grid coated with carbon. Scanning electron microscopy was performed on a FEI (Philips) XL 40 microscope using tungsten filament (200 V–30 keV).

2.3.4. Thermogravimetry

The thermal behavior of the powders was investigated using a Netzsch STA449C thermobalance, with a 10 °C/min heating rate under an argon or air atmosphere.

3. Results and discussion

3.1. Decomposition of uranyl citrate solution

The thermal decomposition of the mixed solutions of uranyl nitrate and citric acid consists of water evaporation, nitrogen and nitrate release as NO_x and citric acid decay into carbon and CO/CO_2/H_2O. The thermogravimetric analysis of a 2.0 mixture (citric acid/uranyl nitrate molar ratio) under Ar in Fig. 3A shows that the main weight loss of an already dried solution is ~45% and it is completed around 500°C. A second weight loss starting at 1200°C corresponds to the onset of the CTR. Fig. 3B presents an oxidation study (in air) of the nanocrystalline UO_2/C sample obtained under Ar. The low temperature weight gain (1→2) corresponds to the oxidation of UO_2 to U_3O_8. The weight loss ~ 11% (2→3) corresponds to the burning of carbon. On this basis the calculated UO_2:C ratio is around 1:3.7.

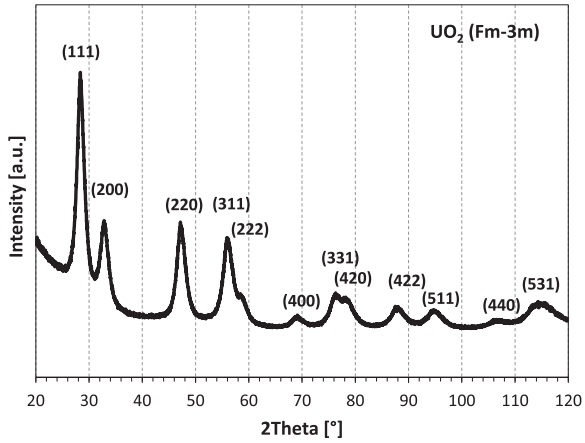

Fig. 5. Powder X-ray diffraction patterns of the UO_2/C nanocomposite obtained at 1000°C from a solution of citric acid and uranyl nitrate with a molar ratio of 2.0. Miller indices of UO_2 ($Fm-3m$) are indicated.

The decomposition product (cit./uranyl ratio of 2.0) in Ar at 1000°C denoted as "nano UO_2/C" was studied by scanning and transmission electron microscopy (Fig. 4). The material consists of porous agglomerates. Nanoparticles of UO_2 with a maximum size of 100nm are embedded in amorphous carbon, which is observable as a thin fuzzy film at the borders of the agglomerates. According to powder X-ray diffraction (Fig. 5) the average crystallite size is

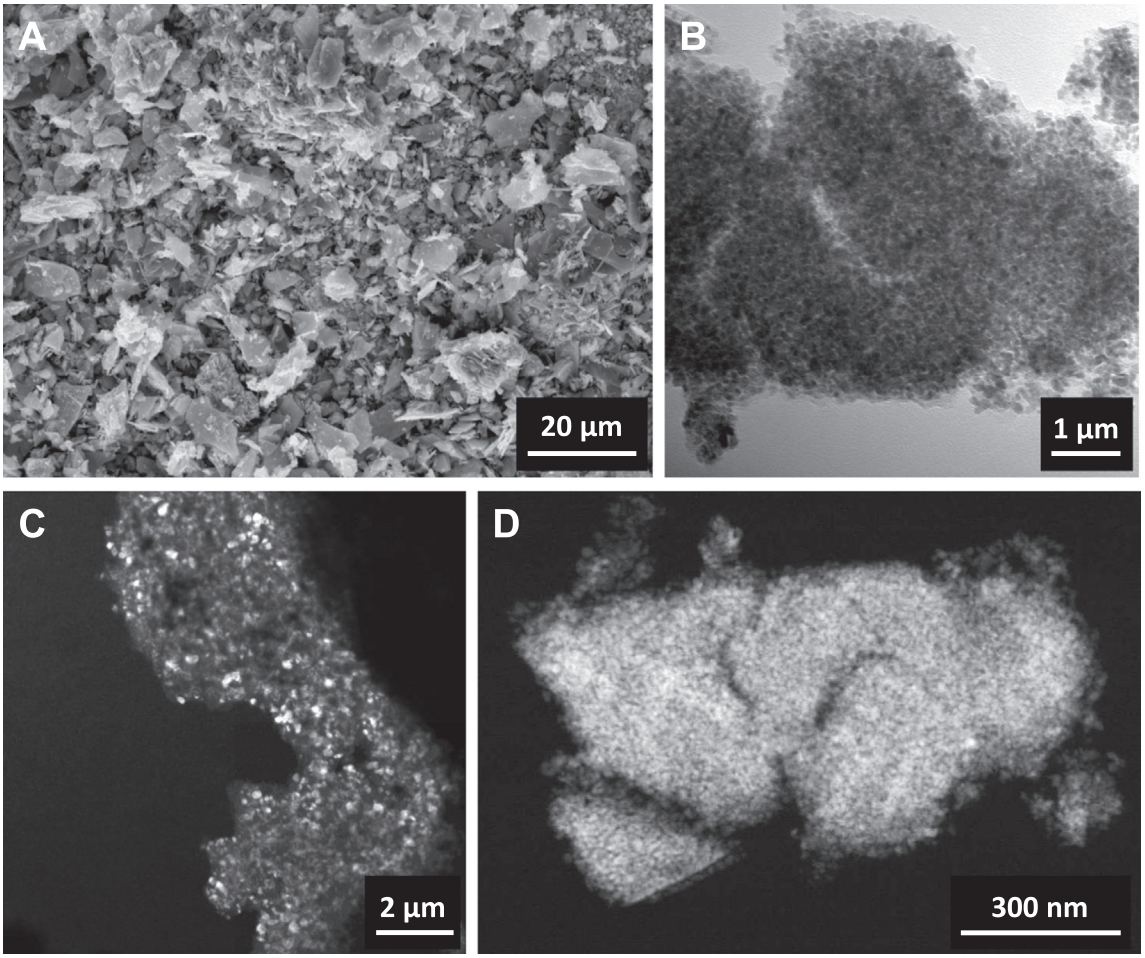

Fig. 4. Electron microscopy of the nanocomposite UO_2/C obtained at 1000°C. The overall morphology by scanning electron microscopy is shown in (A). The crystallites can be seen in the bright (B) and dark field (C) images. The porosity was captured by scanning transmission mode (D).

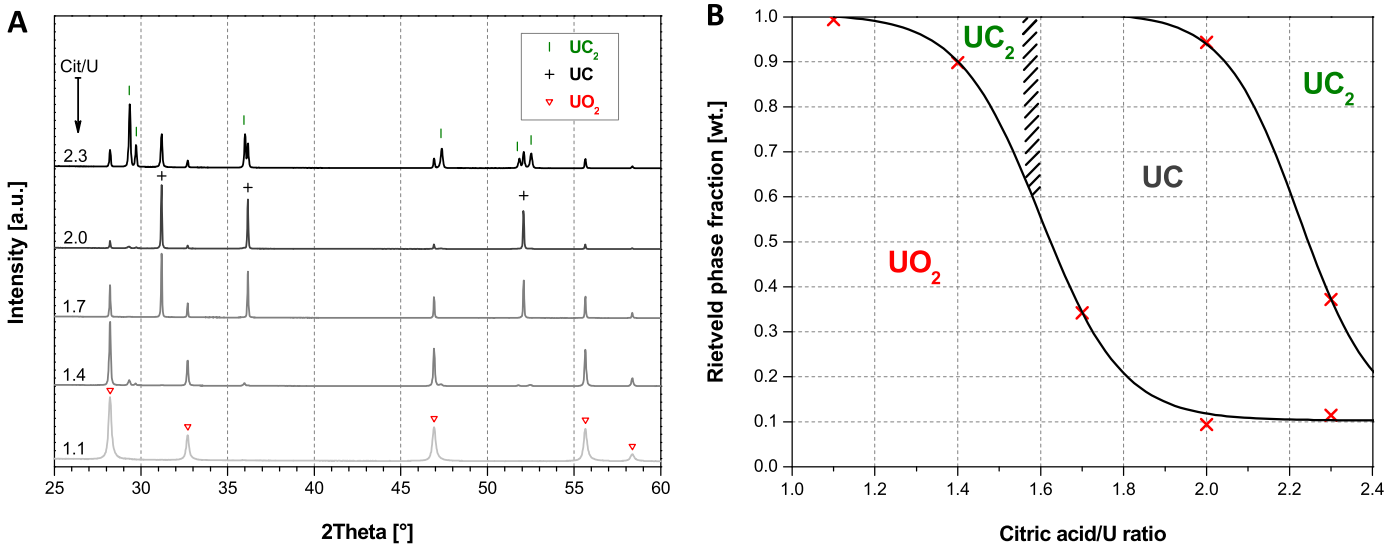

Fig. 6. XRD results of carboreduced UO_2/C nanocomposite at 1600°C for 1h under Argon flow. (A) XRD pattern, "Cit/U" refers to the molar ratio between uranyl ion and citric acid in the initial mixture; (B) Phase proportions deduced from the Rietveld refinement of the data.

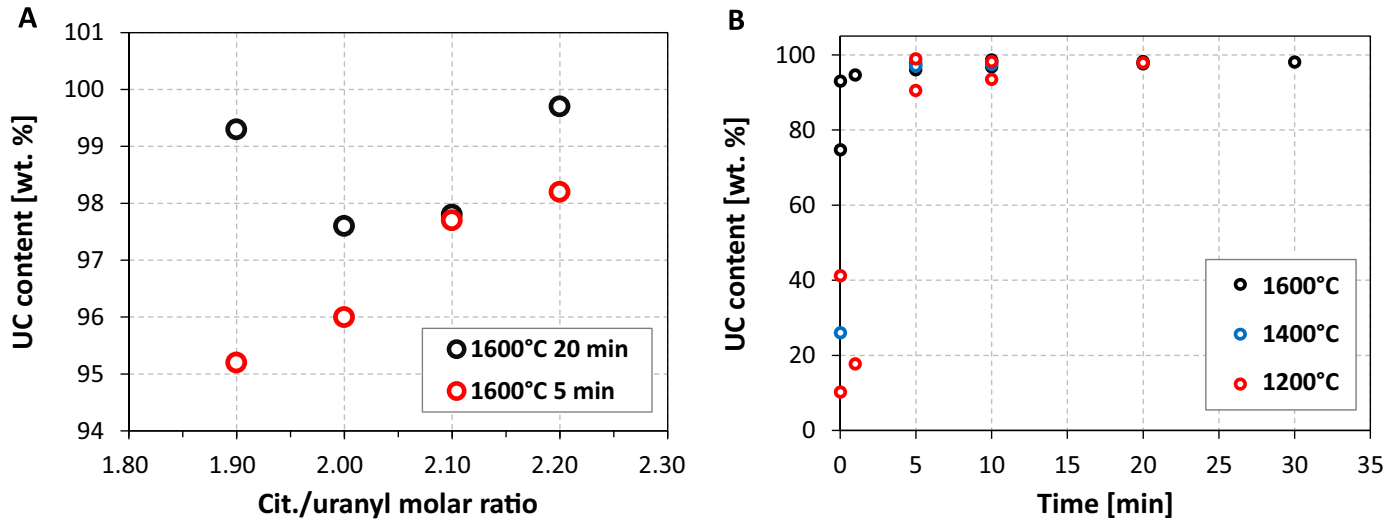

Fig. 7. Study of the UC production using a modified SPS facility. UC content for different citric acid/uranyl nitrate molar ratios received at 1600°C for 5 or 20min (A). Kinetics of the UC formation at 1200, 1400 and 1600°C for a 2.0 ratio (B). The time scale shows the dwell at corresponding temperature.

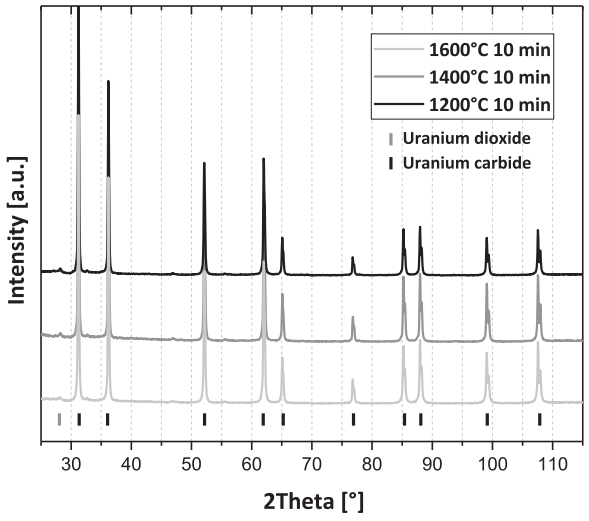

Fig. 8. X-ray diffraction patterns of UC powders obtained in the modified SPS facility at 1200, 1400, 1600°C for 10min.

~10nm with a lattice parameter of 5.435Å, which is significantly lower than the value for $UO_{2.00}$ (5.471Å [27]). Typically, a decrease lattice parameter implies oxygen over-stoichiometric UO_{2+x}, but in this case it could be caused by highly defective structure due to the carbon inclusion in the fluorite lattice as well.

In an attempt to detect the amorphous carbon in the UO_2/C nanocomposite, we hopped to acquire its ^{13}C MAS NMR spectrum. Unfortunately, despite the NMR sensitivity to amorphous phases, no clear signal was obtained here. This is explained because the amorphous phase is not well-known, its signal position cannot be predicted (paramagnetic effect due to the presence of uranium) and also probably because a very broad signal occurs. Further, due to the very low natural abundance of the ^{13}C nuclei (1.1%) and the number of pulses usually required to obtain a spectrum with a minimum resolution, we probably arrived at the limit of this technique.

3.2. Carbothermal reduction in a conventional furnace

For a first optimization of the appropriate ratio between uranyl ion and citric acid initial mixture, a large range of compositions

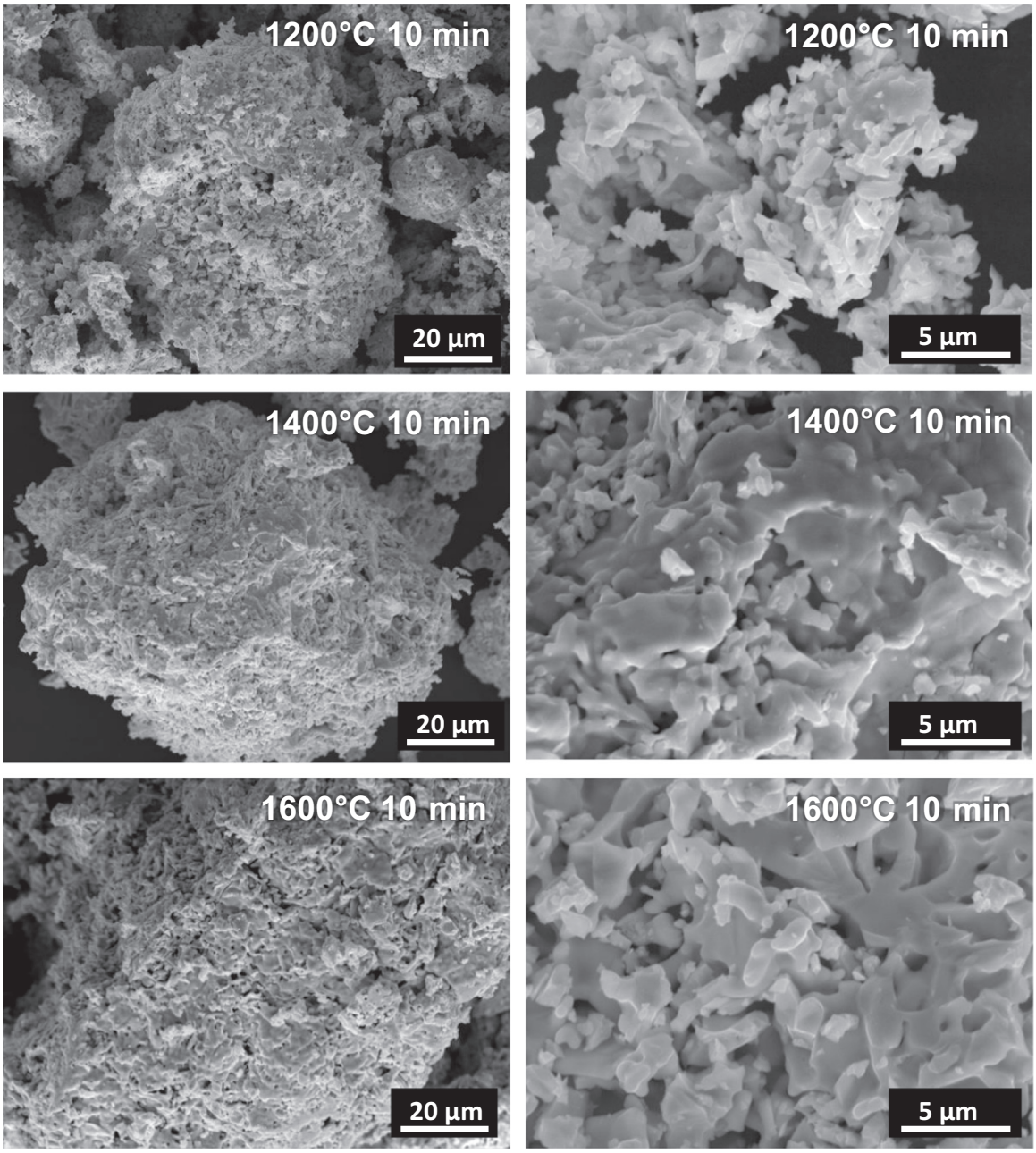

Fig. 9. Scanning electron micrographs of the UC powder after CTR in the modified spark plasma sintering facility. Powders obtained at 1200, 1400 and 1600°C for 10min.

was studied, with citric acid/uranyl ratios going from 1.1 to 2.3. The UO_2/C nanocomposites obtained from the calcination of these were treated one hour at 1600°C under Ar and the resulting powders analyzed by XRD (Fig. 6). A significant amount of uranium carbide appears for a ratio of 1.4. For smaller ratios UO_2 is predominantly formed. For a ratio of 1.4, only the dicarbide UC_2 [28] was observed despite the lack of free carbon available for the CTR. For higher amount of carbon (Cit/U=1.7) UC_2 is not observed anymore and the main phase is UC [29]. These observations seem to be correlated to Eqs. (1) and (2) describing a reaction mechanism in two steps giving first UC_2, and then UC_2 reacting with UO_2 to give UC. The ratio of Cit/U=2.0 gives the best result with 85% of UC and minor amounts of UO_2 and UC_2. Finally, higher amounts of citric acid in the initial mixture lead to an excess of carbon responsible for the increase of UC_2 fraction.

These CTR in a conventional furnace gave promising results for the use of UO_2/C nanocomposite from uranyl/citric acid mixture decomposition to produce uranium carbide. It shows the high reactivity of the precursor, yielding uranium carbide UC in one hour under an argon flow. However, one can see in Fig. 6 that even with an excess of carbon, UO_2 is still present at the 10% level. The presence of UO_2 can be due to UO_2 agglomerate regions in the powder or to a secondary reaction of the powder at high temperature with oxygen impurities in the argon gas. To get a complete reaction, a UO_2/C nanocomposite from Cit/U=2.0 has been pressed into a pellet (200 MPa, zinc stearate lubricant) before CTR in the same conditions. In this case, the final powder contains 96% of UC and 4% of UO_2, and UC_2 was not observed anymore. Further optimizations have not been performed since the main purpose of the study was to produce highly reactive carbide powder for sintering using SPS.

3.3. Carbothermal reduction in the modified SPS facility

The effect of the initial citric acid/uranyl nitrate ratio was studied

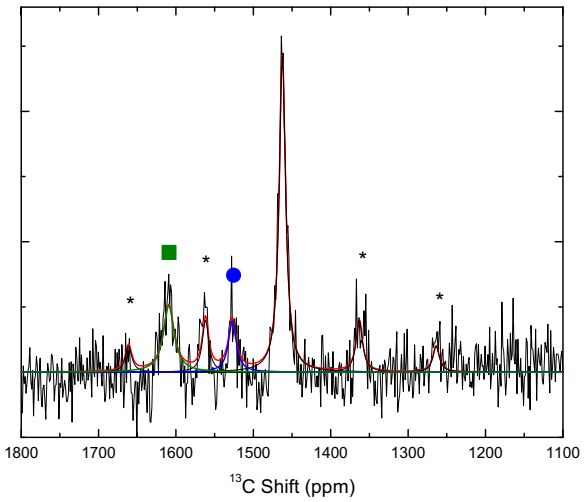

Fig. 10. ^{13}C MAS NMR (10kHz spinning frequency) of the UC powder obtained in the modified SPS facility at 1200°C. Unmarked peak corresponds to the main UC signal. Spinning sidebands are marked with a star. The square and the circle point out secondary signals from the carbide and are discussed in the text.

for a small range of compositions based on the results obtained for CTR in a conventional furnace. It was observed that ratios ≥ 1.9 gave satisfactory UC purity. The results are summarized in Fig. 7A. The tendency to obtain a higher yield of UC with higher carbon content is more visible for samples obtained at 1600°C for 5min. For longer times (20min) the UC yield is generally higher, up to 99.7wt%, but results are scattered with no observable tendency. The kinetic study of the CTR at 1200, 1400 and 1600°C is plotted in Fig. 7B. For all temperatures the reaction yield is over 90% within 5min of reaching of the required temperatures. It means that the CTR has already progressed significantly during the heating ramp (200°C/min) to the desired temperature.

No intermediate UC_2 was observed, it seems that under sufficient vacuum the reaction rate of Eq. (2) is much higher than that of Eq. (1), so the concentration of an intermediate UC_2 is always very small or negligible. Thus, the reaction kinetics would be controlled by the slower step (Eq. (1)), see Fig. 8.

The UC powder morphology as observed by SEM is shown in Fig. 9. It is mostly constituted of spherical porous agglomerates with sizes up to several tens of microns. The individual grain sizes are approximately 1μm for UC powder obtained at 1200°C and above 1μm for higher temperatures. This observation suggests that uranium carbide with increased reactivity can be obtained by limiting the temperature of the CTR. Therefore, the high reactivity of the precursor produced in this study and the efficiency of the modified SPS facility for CTR purpose can be useful to produce carbide more sinter-active.

The ^{13}C MAS NMR spectrum of a UC sample prepared at 1200°C for 10min, acquired at 10kHz, is presented in Fig. 10. Three peaks were identified with one main at 1462ppm (73% of the total intensity) and two others at 1527ppm (blue circle, 10% of the total intensity) and 1609ppm (green square, 17% of the total intensity). Compared to the previous NMR results obtained on UC_x compounds, [30,31] the main peak clearly indicates the presence of $UC_{1.00}$ in the sample. The peak at 1527ppm was also previously identified and attributed to carbon defects. The last peak corresponds to a new C species which was not observed in $UC_{1.00}$ obtained with the arc melted technique. This additional carbon could be surrounded by O atoms [32].

4. Conclusion

We report a simple and efficient preparation route for uranium carbide. Carbothermal reduction using nanocomposites of UO_2 and carbon as a starting material has been tested under conventional conditions and in a modified spark plasma sintering facility. In a conventional furnace using argon atmosphere the nano UO_2/C powder gave uranium carbide of high purity at 1600 °C for a 1 h dwell time. A UC_2 intermediate was observed in this case. The citric acid/uranyl nitrate ratio of 2.0 in the initial mixture seems to be the most appropriate for UC synthesis. The yield of CTR has been found to be critically sensitive to the partial pressure of CO. In a modified spark plasma sintering set-up (under vacuum) the CTR occurs under mild conditions, 1200 °C within 5 min. Thanks to the fast heating/cooling ramps of the SPS facility the produced powder is fine-grained and therefore more sinter-active. Sintering of such powders will be a part of future studies. No UC_2 intermediate was observed during the CTR in the SPS facility, which we attribute to the high vacuum and easy release of CO. Thus, the reaction in Eq. (2) is either fast or different reaction mechanism takes place.

Acknowledgments

We are thankful to Daniel Bouexière and Olaf Walter for XRD analysis, Christian Berkmann for the modified SPS die and punches design, Bert Cremer for SEM analysis and Herwin Hein for thermogravimetric analyses. We are also thankful to Co Boshoven and Michael Holzhäuser for their support during sample preparation.

References

[1] A.K. Sengupta, R. Agarwal, H.S. Kamath, 3.03 - carbide fuel A2 - konings, in: J.M. Rudy (Ed.), Comprehensive Nuclear Materials, Elsevier, Oxford, 2012, pp. 55–86, http://dx.doi.org/10.1016/B978-0-08-056033-5.00051-3.
[2] D. Manara, F. De Bruycker, A.K. Sengupta, R. Agarwal, H.S. Kamath, 2.04 - Thermodynamic and thermophysical properties of the actinide carbides A2 - konings, in: J.M. Rudy (Ed.), Comprehensive Nuclear Materials, Elsevier, Oxford, 2012, pp. 87–137, http://dx.doi.org/10.1016/B978-0-08-056033-5.00011-2.
[3] A. Fernandez, J. McGinley, J. Somers, M. Walter, Overview of past and current activities on fuels for fast reactors at the Institute for Transuranium Elements, J. Nucl. Mater. 392 (2009) 133–138, http://dx.doi.org/10.1016/j.jnucmat.2009.03.006.
[4] Y. Suzuki, T. Sasayama, Y. Arai, H. Watanabe, Fabrication of uranium-plutonium mixed carbide pellets, J. Nucl. Sci. Technol. 18 (1981) 61–70, http://dx.doi.org/10.1080/18811248.1981.9733223.
[5] C. Ganguly, P.V. Hegde, G.C. Jain, Fabrication of $(Pu_{0.55}U_{0.45})C$ fuel pellets for the second core of the fast breeder test reactor in India, Nucl. Technol. 105 (1994) 346–354 ⟨http://www.ans.org/pubs/journals/nt/a_34935⟩.
[6] C. Duguay, G. Pelloquin, Fabrication of mixed uranium–plutonium carbide fuel pellets with a low oxygen content and an open-pore microstructure, J. Eur. Ceram. Soc. 35 (2015) 3977–3984, http://dx.doi.org/10.1016/j.jeurceramsoc.2015.05.026.
[7] S. Vaudez, C. Riglet-Martial, L. Paret, E. Abonneau, GEN IV: Carbide Fuel Elaboration for the 'Futurix Concepts' experiment, IYNC 2008: International Youth Nuclear Congress 2008, 2008, pp. 568–573, ⟨http://www.iaea.org/inis/collection/NCLCollectionStore/_Public/40/048/40048093.pdf⟩.
[8] B. Matović, B. Babić, D. Bučevac, M. Čebela, V. Maksimović, J. Pantić, M. Miljković, Synthesis and characterization of hafnium carbide fine powders, Ceram. Int. 39 (2013) 719–723, http://dx.doi.org/10.1016/j.ceramint.2012.06.083.
[9] C. Yan, R. Liu, C. Zhang, Y. Cao, Zirconium carbide, hafnium carbide and their ternary carbide nanoparticles by an in situ polymerization route, RSC Adv. 5 (2015) 36520–36529, http://dx.doi.org/10.1039/C4RA14996C.
[10] D. Lu, W. Wang, H. Wang, J. Zhang, Y. Wang, F. Zhang, Z. Fu, Synthesis of ultrafine hafnium carbide powders combining the methods of liquid precursor conversion and plasma activated sintering, Ceram. Int. 42 (2016) 8108–8114, http://dx.doi.org/10.1016/j.ceramint.2016.02.012.
[11] Y. Chen, H. Zhang, H. Ye, J. Ma, A simple and novel route to synthesize nano-vanadium carbide using magnesium powders, vanadium pentoxide and different carbon source, Int. J. Refract. Met. Hard Mater. 29 (2011) 528–531, http://dx.doi.org/10.1016/j.ijrmhm.2011.03.004.
[12] A. Sinha, T. Mahata, B.P. Sharma, Carbothermal route for preparation of boron carbide powder from boric acid–citric acid gel precursor, J. Nucl. Mater. 301 (2002) 165–169, http://dx.doi.org/10.1016/S0022-3115(02)00704-3.
[13] T. Onoki, Y. Ueoka, B. Xu, N. Shiota, Y. Naganuma, A. Matsuoka, Y. Minamibori, T. Tagami, Synthesis and classification of WC and W metals via organic-

inorganic complex precursors, J. Ceram. Soc. Jpn. 121 (2013) 572–574, http://dx.doi.org/10.2109/jcersj2.121.572.
[14] C. Yan, R. Liu, Y. Cao, C. Zhang, D. Zhang, Synthesis of zirconium carbide powders using chitosan as carbon source, Ceram. Int. 39 (2013) 3409–3412, http://dx.doi.org/10.1016/j.ceramint.2012.09.032.
[15] M. Brykala, M. Rogowski, T. Olczak, Carbonization of solid uranyl-ascorbate gel as an indirect step of uranium carbide synthesis, Nukleonika 60 (2015) 921–925, http://dx.doi.org/10.1515/nuka-2015-0122.
[16] B. Li, Y.-C. Song, C.-R. Zhang, J.-S. Yu, Synthesis and characterization of nanostructured silicon carbide crystal whiskers by sol–gel process and carbothermal reduction, Ceram. Int. 40 (2014) 12613–12616, http://dx.doi.org/10.1016/j.ceramint.2014.04.099.
[17] H. Muta, K. Kurosaki, M. Uno, S. Yamanaka, Thermal and mechanical properties of uranium nitride prepared by SPS technique, J. Mater. Sci. 43 (2008) 6429–6434, http://dx.doi.org/10.1007/s10853-008-2731-x.
[18] D. Liu, W.-F. Qiu, T. Cai, Y.-n Sun, A.-J. Zhao, T. Zhao, Synthesis, characterization, and microstructure of ZrC/SiC composite ceramics via liquid precursor conversion method, J. Am. Ceram. Soc. 97 (2014) 1242–1247, http://dx.doi.org/10.1111/jace.12876.
[19] J.J. Lenhart, S.E. Cabaniss, P. MacCarthy, D. Honeyman Bruce, Uranium(VI) complexation with citric, humic and fulvic acids, Radiochim. Acta 88 (2000) 345, http://dx.doi.org/10.1524/ract.2000.88.6.345.
[20] E.H. Bailey, J.F.W. Mosselmans, P.F. Schofield, Uranyl-citrate speciation in acidic aqueous solutions—an XAS study between 25 and 200 °C, Chem. Geol. 216 (2005) 1–16, http://dx.doi.org/10.1016/j.chemgeo.2004.10.011.
[21] Y. Suzuki, Y. Arai, T. Sasayama, H. Watanabe, Kinetics on carbothermic reduction of UO2+C powders and compacts to UC2, J. Nucl. Sci. Technol. 19 (1982) 222–230, http://dx.doi.org/10.1080/18811248.1982.9734137.
[22] V. Tyrpekl, C. Berkmann, M. Holzhäuser, F. Köpp, M. Cologna, T. Wangle, J. Somers, Implementation of a spark plasma sintering facility in a hermetic glovebox for compaction of toxic, radiotoxic, and air sensitive materials, Rev. Sci. Instrum. 86 (2015) 023904, http://dx.doi.org/10.1063/1.4913529.
[23] L. Feng, S.-H. Lee, H. Wang, H.-S. Lee, Synthesis and densification of nanocrystalline hafnium carbide powder, J. Eur. Ceram. Soc. 35 (2015) 4073–4081, http://dx.doi.org/10.1016/j.jeurceramsoc.2015.08.004.
[24] V. Petříček, M. Dušek, L. Palatinus, Crystallographic computing system JANA2006: general features, Z. Krist. 229 (2014) 345–352, http://dx.doi.org/10.1515/zkri-2014-1737.
[25] L. Martel, J. Somers, C. Berkmann, F. Koepp, A. Rothermel, O. Pauvert, C. Selfslag, I. Farnan, A nuclear magnetic resonance spectrometer concept for hermetically sealed magic angle spinning investigations on highly toxic, radiotoxic, or air sensitive materials, Rev. Sci. Instrum. 84 (2013) 055112, http://dx.doi.org/10.1063/1.4805017.
[26] D. Massiot, F. Fayon, M. Capron, I. King, S. Le Calvé, B. Alonso, J.-O. Durand, B. Bujoli, Z. Gan, G. Hoatson, Modelling one- and two-dimensional solid-state NMR spectra, Magn. Reson. Chem. 40 (2002) 70–76, http://dx.doi.org/10.1002/mrc.984.
[27] G. Leinders, T. Cardinaels, K. Binnemans, M. Verwerft, Accurate lattice parameter measurements of stoichiometric uranium dioxide, J. Nucl. Mater. 459 (2015) 135–142, http://dx.doi.org/10.1016/j.jnucmat.2015.01.029.
[28] U. Carvajal Nuñez, R. Eloirdi, D. Prieur, L. Martel, E. López Honorato, I. Farnan, T. Vitova, J. Somers, Structure of UC_2 and U_2C_3: XRD, ^{13}C NMR and EXAFS study, J. Alloy. Compd. 589 (2014) 234–239, http://dx.doi.org/10.1016/j.jallcom.2013.11.202.
[29] N. Vigier, C. Den Auwer, C. Fillaux, A. Maslennikov, H. Noël, J. Roques, D. K. Shuh, E. Simoni, T. Tyliszczak, P. Moisy, New data on the structure of uranium monocarbide, Chem. Mater. 20 (2008) 3199–3204, http://dx.doi.org/10.1021/cm8001783.
[30] W.B. Lewis, S.W. Rabideau, N.H. Krikorian, W.G. Witteman, Knight shifts of C13 in the carbides of uranium and thorium, Phys. Rev. 170 (1968) 455–462, http://dx.doi.org/10.1103/PhysRev.170.455.
[31] U. Carvajal Nuñez, L. Martel, D. Prieur, E. Lopez Honorato, R. Eloirdi, I. Farnan, T. Vitova, J. Somers, Coupling XRD, EXAFS, and ^{13}C NMR to study the effect of the carbon stoichiometry on the local structure of UC1 ± x, Inorg. Chem. 52 (2013) 11669–11676, http://dx.doi.org/10.1021/ic402144g.
[32] K. Maruya, Oxygen in uranium carbide during carbothermic reduction processes, J. Nucl. Sci. Technol. 7 (1970) 13–18, http://dx.doi.org/10.1080/18811248.1970.9734634.